The Effect of the Multi-doping Strategy on Stabilization of the Cubic δ-phase in the Bi2O3-based Solid Electrolyte Systems in Terms of the SOFC Applications

Murat BALCI (muratbalci@erciyes.edu.tr)
Erciyes University: Erciyes Universitesi https://orcid.org/0000-0003-1297-1691
Mehmet Arı
Erciyes University: Erciyes Universitesi
Yasin Polat
Nevsehir University: Nevsehir Haci Bektas Veli Universitesi

Research Article

Keywords: Solid electrolyte, Phase stabilization, Ion conductivity, Activation energy, X-ray Diffraction, Solid state reactions

Posted Date: December 28th, 2021

DOI: https://doi.org/10.21203/rs.3.rs-1161650/v1

The Effect of the multi-doping strategy on stabilization of the cubic δ-phase in the Bi_2O_3-based solid electrolyte systems in terms of the SOFC applications

[a]Murat Balci, [b]Mehmet Arı, [c]Yasin Polat

a Department of Physics, Erciyes University, 38039 Kayseri, Turkey
b Department of Physics, Erciyes University, 38039 Kayseri, Turkey
c Science and Technology Application and Research Center, Nevşehir Hacı Bektaş Veli University, 50300 Nevşehir, Turkey

ABSTRACT

In this study, the effects of multi-doping strategy on phase stabilization and electrical conductivity for the doped Bi_2O_3 system were investigated. All solid mixtures were created by solid state reactions according to a certain stoichiometric ratio in atmospheric conditions. The structural, electrical, thermal and surface characterizations of the created samples were performed by x-ray diffraction method (XRD), four point-probe technique (4-PPT), differential thermal analysis/thermo gravimetric analysis (DTA/TGA) and scanning electron microscope (SEM), respectively. From XRD results, it was seen that the fcc δ-phase could be stabilized by using only 1:1:1:2 or 2:2:2:1 dopant content ratio (in here, "1:" is corresponds to" 5%" mole). The other compounds prepared out of this ratios were mixed phase because of the containing both α-phase peaks and δ-phase peaks on their XRD pattern. When the all samples were compared in terms of electrical conductivity at 750 °C, it was observed that the fcc δ-phase stabilized samples exhibited higher conductivity than that of other compounds as expected. The highest electrical conductivity was for the sample, dopant content ratios of which are 1: 1: 1: 2, with 0.014 $S.cm^{-1}$ at 750 °C and also it had the lowest activation energy (0.51 eV) among all samples. On the other hand, according to the thermal analysis results, it was concluded that phase transition occurred only on the DTA curve of the sample given with dopant content ratios 1:1:1:1 due to presence of endothermic peak on its DTA curve at 729°C during the heating process. Also, for this sample, it was clearly predicted from the electrical conductivity graphs depending on temperature that the phase transition occurred at just that temperature (729 °C) due to the sudden increase in conductivity by indicating phase transition from the α-phase to the cubic δ-phase. The SEM analysis pointed out that grain size decreased as total dopant ratio increased and also the grain boundary changed sharply with the increase in the total dopant ratio.

Keywords: Solid electrolyte; Phase stabilization; Ion conductivity; Activation energy; X-ray Diffraction; Solid state reactions.

1. Introduction

In recent years, the attention to solid oxide fuel cells (SOFCs) as an alternative energy source has considerably increased due to its notable features such as highly electrical efficiency, eco-friendly in terms of harmful waste gasses compared to fossil fuels [1, 2]. At the high operating temperature (>800°C), the SOFCs units may encounter a number of problems that reduce cell performance, as an illustration, the material corrosion between cell components may cause a decrease in electrical efficiency. Also besides that, the high temperature solid oxide fuel cells (HT-SOFCs) can only be used in built-in power units such as hospitals and power plants due to the its high operation temperature [3]. For this reason, the reducing operating temperature of SOFCs to lower temperatures (<650°C) can help to overcome the problems that arise as a result of the high operating temperature. However, it has been observed by many researchers that the cell kinetic reactions between electrodes-electrolyte in SOFCs units, in which the Yttria-stabilized zirconia (YSZ) type electrolyte commonly is used, have dramatically slowed down together with the decrease in ionic conductivity of electrolyte as a result of the reduction in operating temperature.

On the other hand, as an alternative to YSZ electrolytes, the Bi_2O_3-based solid electrolyte system, which exhibits higher oxygen ion conductivity compared to YSZ materials at all temperatures, is being studied intensively. [4, 5]. But the cubic δ-phase with the highest ion conductivity is referred to as the metastable phase due to its stability in the range of 729 °C - 824 °C. Accordingly, the many researchers have mainly tried to stabilize the δ-Bi_2O_3 by doping the some lanthanide oxides into pure-Bi_2O_3 crystal [6-14]. As a common result of all these studies, it was clearly observed that the ionic conductivity of stabilize cubic δ-phase was less than that of the pure cubic phase despite the achieving phase stability of the δ-phase at all temperatures. The decaying in conductivity is usually attributed to difference in the polarizability between host and dopant cation in which the polarizability of Bi^{3+} is higher than from that of the dopant cation owing to lone pair of $6s^2$ electrons [15- 16]. That's why, the polarizability degree of dopant cation may seem important in terms of the compensating for the decaying in conductivity [17].

As for the phase stabilization of the cubic δ-Bi_2O_3, especially, when dopants having smaller radii than that of host Bi^{3+} cation was used, it was emphasized that δ-phase could be easily stabilized due to the preventing phase transition to monoclinic α-phase through the lattice shrinking. Also, in literature, when the single and double-doped Bi_2O_3 electrolytes were compared in terms of the electrical conductivity and the phase stabilization, it was pointed out that double-doped systems provided both higher ion conductivity and easier phase stabilization. Wachsman et al.'s explained that compound

$(BiO_{1.5})_{0.88}$ $(DyO_{1.5})_{0.08}(WO_3)_{0.04}$ had the higher ion conductivity (0.57 S/cm at 800 °C) than single doped systems such as erbium stabilized bismuth oxide (20ESB), the conductivity of which is the highest among single systems with 0.38 S/cm at 800 °C [18]. According to this study, the reason for the high ion conductivity in double-doped systems was to use dopants, the polarizability of which is closest to that of bismuth, by taking into account other parameters such as dopant type and rate, annealing temperature. Besides, they particularly suggested that the total doping rate should be fixed to 12% in order to both to stabilize the cubic δ-phase more easily and to compensate for the decrease in ion conductivity as a result of the decrease in cation polarizability. Swagata et al. also have dealt with the double-doping strategy by fixing total dopant ratio to 12% just like Wachsman et al. and they used Dy and Ho as dopants for stabilization of cubic δ-phase [19]. According to results obtained from this study, they achieved to stabilize cubic δ-phase at all temperatures and they found that the ion conductivity was 0.57 $S.cm^{-1}$ at 700 °C, which was the highest ion conductivity among all binary systems studied in the literature. Similarly, Yılmaz et al.'s also studied double-doped system in which they used Dy and Yb as dopants and they found that the conductivity was quite close to Wachsman's results with 0.51 S/cm for 14Yb10DSB mixture at 800 °C, although they exceeded 12% total doping rate suggested by Wachsman et al. for double-doped systems [20-21].

In this study, we wondered that whether or not there is a limitation in terms of the dopant number to achieve stabilization of the cubic δ-phase of Bi_2O_3 at all temperatures. For this purpose, we employed four lanthanide oxides (Ln_2O_3, Ln = Er, Eu, Gd and Ho) as dopant material in order to stabilize the cubic δ-phase from high temperature to room temperature. The cation radius was chosen smaller than that of host Bi^{+3} cation (1.17 Å) to stabilize the cubic phase easily by obstructing any phase transition to other phases by means of lattice shrinkage. Because of its high polarizability among others, in mixture, the holmium was used as main dopant and its dopant rate was fixed at a certain rate, while others were changed. In this way, we hope to achieve both phase stability by using smaller cation radius and compensate for the dramatic drop in ion conductivity owing to high polarizability of the holmium. The mixture having lowest doping rate was prepared by fixing the total dopant rate to 20% in which its abbreviation was denoted by 1:1:1:1 (in here, "1:" corresponds to "5% "mole) and also other mixtures were created by varying the dopant ratios according to a certain stoichiometry.

2. Experimental Procedure

The Nano powders consisted of the Bi_2O_3 (% 99,99 purity, Sigma Aldrich), Gd_2O_3 (%99,98 purity, Sigma Aldrich), Eu_2O_3 (%99,97 purity, Sigma Aldrich), Er_2O_3 (%95,99 purity, Sigma Aldrich) and Ho_2O_3 (%96,99 purity, Sigma Aldrich). All mixtures in this study were created by solid state reactions under atmospheric conditions by following certain stoichiometry. The total dopant ratio in mixture was changed from 20% to 80% to observe how crystal structure and ion conductivity will be affected by dopant ratio increase. As for the dopant content ratios in mixture, Ho was selected as main dopant, the polarizability of which is higher than that of the other lanthanides, and mole ratios of the other lanthanides were equally changed step by step up to 20 % by 5% increase. Afterwards, the mass values corresponding to mole ratios for the each -oxide in the mixture were measured by via digital precision scale and then, in order to achieve nano powder mix, the all powders were slowly grounded by the aid of a pestle in an agate mortar. To carry out some experimental studies such as electrical conductivity measurements, a small portion of the powder mixes was used for prepare pallet samples having 13 mm diameter and 5 mm thickness. The pallets were created by pressing-machine, which can apply approximate 10 tons press on powders in axial position. After sample preparation, all samples were subjected to heat treatment in order to achieve stabilization of the cubic δ-phase for all operating temperatures. That's why, the annealing temperature in this study were determined as 750 °C, which is a temperature above the phase transition temperature (729 °C) from the cubic δ-phase to the α-phase. Also, the annealing time was set to 100 hours to ensure good solidification and phase stabilization.

The microstructure analysis of the annealed samples were performed by x-ray diffraction technique (XRD) in order to observe whether phase stabilization was achieved or not, as well as uncovering some crystal parameters such as unit cell parameter and crystal size. Besides, the XRD analyses for all samples were carried out with Bruker AXS D9 Advance type diffractometer at room temperature by using Cu-Kα radiation the having 1.54 Å wavelength. Also, the scanning step was chosen as $0.02°sec^{-1}$ from 10° to 90°.

The thermal characterizations for all samples were examined by Diamond TG/DTA-Perkin Almer Marck system to uncover whether phase transition and mass loss or not the depending on temperature. In this system, the heating rate was fixed to 10 $°min^{-1}$ to precisely observe endothermic or exothermic peaks indicating a potential phase transition on the

DTA curves. The surface analysis for all samples were carried out by Leo 440 model Scanning Electron Microscope (SEM) to observe some the surface features such as grain size, grain connectivity.

Finally, the electrical conductivities of all samples were measured by Four Point Probe Technique (4PPT) in where the resistivity can be accurately measured without any additional resistivity such as contact resistance. The measurements were carried out through an alumina kit system in a programmable ash furnace by using the multimeter (Keithley 2700) with a D.C power source (Keithley 2400). In here, the furnace temperature was slowly increased from room temperature to high temperature (1000 °C) with a constant heating step (10 °C.min^{-1}) throughout measurement.

3. Results and Discussions

3.1. Microstructure Analysis

The XRD profiles for some annealed samples were overlapped in Fig. 1 to observe stabilization of the δ-phase at room temperature. From this figure, we can clearly see that the cubic δ-phase has been stabilized for only two samples, the dopant content ratios of which are given by 1:1:1:2 and 2:2:2:1, due to taking part of only the δ-phase peaks on their XRD pattern. According to this results, it can be said that the cubic δ-phase can be stabilized more easily by using 2:2:2:1 or 1:1:1:2 dopant content ratios as similar to previous studies carried out by Jung et al [22]. As for other compounds doped by different dopant content, it was also observed that the α-peaks together with the δ-peaks occurred on their pattern. Thus, it can clearly be inferred that all of them have a heterogeneous phase due to the presence of both δ-(cubic) and α-(mono) peaks on their XRD patterns.

On the other hands, the peak broadening, which indicates an increase in crystal defect density in the lattice, was observed on the XRD pattern as the total doping ratio increases while the average crystal size decreased [23]. These defects may be generally originated from the misplacement of the dopant cations in the lattice due to excessive doping (>35%) as well as the polarizability effects of each cation in lattice. Also, as can be clearly seen from Fig. 1, the density of the α-peaks referring to the formation of many crystal clusters increased with increasing total doping rate in mixture. Especially, the sample having total doping rate of 50% exhibits multi-phase structure, the peak width of which is considerably larger than that of others. As a result, it can be said that the peak broadening is closely related to the increase in the doping rate and the density of the α-peaks on the pattern [24]. The average crystal size of particles was calculated by Scherrer-Warren equations thanks to “X-Powder” data processing program in which equations is given by

$$D = \frac{0.9\lambda}{\beta_{hkl} cos\theta_{hkl}} \quad (1)$$

In where, λ is the wavelength of the x-rays, θ_B is the Bragg diffraction angle, D is the average crystallite size and β represents the FWHM line broadening, which is calculated from Eq. (2).

$$\beta^2 = \beta_m^2 - \beta_s^2 \quad (2)$$

In Eq. (2), β_m is the corrected FWHM value and β_s represents the contribution from reflections. The FWHM values were calculated over the main peak at 28.8° (111) on the pattern and also the other microstructure parameters such as dislocation density and microstrain is given by following equations.

$$\varepsilon = \frac{\beta_{hkl}}{4tan\theta_{hkl}} \quad (\textit{Lattice Microstrain}) \quad (3)$$

$$\delta = \frac{1}{D^2} \quad (\textit{Dislocation density}) \quad (4)$$

In Eq. 3, ε is the microstrain closely related to the lattice strain, β_{hkl} is the fwhm value of the strongest peak on the diffraction pattern and θ_{hkl} is the Bragg angle at which the strongest peak on the diffraction pattern occurs. Other hand, In Eq. 4, δ is the dislocation density and D is the crystal size in nanometer. When Eq. (3) and Eq. (1) are

In Fig. 2(a), the change of FWHM and d-spacing values according to the average crystal size is shown. From the figure, as can be clearly seen that the increase in the total doping rate resulted in higher Fwhm value as a result of peak broadening. Also, it can be emphasized that the loss of peak sharpness or peak splitting brought about the decreasing in the average crystal size varying inversely with Fwhm value [25]. Thus, the distance between sequential two lattice planes called by d-spacing decreased as the total dopant ratio in mixture increased. This station may be due to an increase in dislocation density in lattice with increasing total dopant rate [26]. According to table 1 and Fig. 2(b), it can be said that the microstrain increased due to the increase in dislocation density as a result of the increase in the total dopant ratio. Thus, it can be seen that as the lattice microstrain in the crystal increases, the average crystal size (D) decreases together with d-spacing called by the distance between the lattice planes.

On the other hand, it can be clearly seen from the Fig. 2(a), the sample labelled by 4: 4: 4: 3, the total dopant ratio of which is equal to 65%, has the highest FWHM value among samples given on the figure as well as the lowest crystal size and with the highest dislocation density. This decrease in average crystal size resulting from an increase in the total dopant ratio can be attributed to occurring the different polarization points, which can effects arrangement of the lattice planes.

Hence, the crystal size of particles may have decreased as a result of the occurring of many different crystal clusters in lattice with doping. Similarly, the XRD profile of the sample prepared with 50% total dopant ratio, in which its dopant content ratios are given by 2:2:2:4, shows that it is mixed phase due to containing the α-phase together with the δ-phase peaks. Therefore, the Fwhm of it is larger than samples prepared with lower ratio and thus, the density of the α-phase peaks on its XRD pattern is more than that of the others. The lattice constants, which are specified in the Table 1, are smaller than that of pure δ-phase due to using smaller cation radii than host Bi^{3+} cation as similar to previous studies carried out on the phase stabilization of the cubic δ-phase [27- 29]. Additionally, when the lattice constant of the samples containing only the δ-phase peaks compared to each other, the unit cell parameter increased as the mole ratio of the Ho, the cation radii of which is larger than other dopants, increased.

3.2. Conductivity and Thermal Analyses

The electrical conductivities of the annealed samples were measured by Four Point Probe Technique (4-FPPT) from room temperature to high temperature (~1000°C) in the programmable furnace. Fig. 3(a) shows the conductivity change depending on temperature of the sample, the total dopant ratio of which is 20%. From the Fig. 3(a), as can be seen that two different conductivity regime formed on the graph due to the crystal structure transformation, which is generally known as a phase transition from α-phase to δ-phase at ~730 °C. Also, at that temperature, it can be observed that the electrical conductivity suddenly begins to increase because of the lower activation energy (0.32 eV) in high temperature region compared to low temperature region. Besides, this discontinuity on the conductivity graph did not occur in any of the other samples and thus, it indicates that no phase transition occurred in any of them, which consistent with the DTA results.

As a comment, we can say that the electrical conductivity began to increase sharply at that temperature on the graph the since low activation energy facilitated the movement of mobile oxygen ions towards the vacant ion centers in the lattice. Fig. 3(b) shows the conductivities comparisons of the samples having different dopant ratios in the certain temperature range (600 °C - 850 °C). As can be clearly seen from the figure that the electrical conductivity decreased with the increase in total dopant ratios. Also, the electrical conductivities changed linearly in accordance with the Arrhenius equation as follows:

$$\sigma_T = \sigma_0 e^{-\frac{E_A}{kT}} \tag{5}$$

where, σ_T is the conductivity at the certain temperature, σ_0 is the pre-exponential factor, k_B is the Stefan-Boltzmann constant and E_A is the activation energy. The conductivity plots were also used to calculate the activation energies of samples by taking a slope on the graph within the specified temperature range.

According to the table 2, it can be said that the highest conductivity among all mixtures was belonged to the sample specified by 1:1:1:2 at 750 °C, which was predicted to be the δ-phase according to XRD result of it. Also, from the table, as activation energies increased, the electrical conductivity decreased as expected due to the restriction of the ion conduction pathways in which the mobile oxygen ions can easily move in lattice [30]. It can be imaginable that the using multi-dopants might have created the new trapping centers, which allows the formation of a short-range ordering for oxygen ions, in lattice. Therefore, not all of the mobile oxygen ions could continue to move through ion voids in lattice anymore because of the existence of this trapping centers [31- 32].

The thermal analysis of all samples were performed by Perkin Elmer DTA/TGA system in between room temperature and 1000 °C with 10 °C.min^{-1} heating rate. Fig .4(a) shows DTA and TGA curves for the samples having different dopant contents. On this figure, as can be clearly seen that an endothermic peak at 729 °C, which indicates phase transition from the α-phase to the δ-phase, occurred on the DTA curve of the sample, the dopant content ratios of which are given by 1: 1: 1: 1 [33- 34]. As for DTA curves of other samples, it is observed that no exothermic or endothermic peaks formed on their DTA curves due to single δ-phase. On the other hand, the TGA curve of the sample containing endothermic peak shows that mass loss during the heating process is negligible because of the very small fluctuations on the its TGA curve. From Fig. 4(b), it can be inferred that the electrical conductivity of the samples decreased as the doping rate increased in mixture. As a reason for the dramatic drop in electrical conductivity, the multi-doping strategy can be considered due to deterioration of the crystal structures together with the high doping rate. Besides, the ratio of components in the mixture can effect transference of mobile oxygen ions to vacant ion centers in sublattice due to different the polarizability degree of each dopant in mixture.

3.3. Surface characterization

The SEM images taken at room temperature of the annealed samples are shown in Fig. 5. In Fig. 5(a), the SEM image of the sample doped by the lowest dopant ratio is showed, in which the connectivity of grains and the grain distribution is not uniform but without any porous structure, which can negatively effects the electrical conductivity. On the other hand,

when the total dopant rates were changed, it was observed that grain boundary structure and shape of grains turned into from a pea view to a polygonal view accompanied by the increase in the number of pores. In Fig. 5(d), the SEM image of the sample doped by 50% showed that the particle size was smaller than that of the Fig. (a), (b) and (c). Therefore, it can be thought that the shrinkage in particle size also leads to a decrease in the average crystal size calculated in microstructure analysis. Also, it can be interpreted from this image that an increase in porosity can play an important role in decreasing electrical conductivity because of the blocking of ion transfer paths. Thus, when the SEM images given in Fig. 5(a), which has the lowest number of poles, is evaluated together with the electrical conductivity results, it can be said that it has the higher conductivity among other samples given in Fig. 5.

4. Conclusions

As a result from this study, we can say that the dopant number used for stabilization and doping rate is very important for achieving stabilization of the fcc δ-phase at all operating temperatures in terms of the SOFCs applications. We found that dopant ratios should be chosen as 1: 1: 1: 2, as previously suggested by some researchers [35-36], otherwise, it was seen that the samples had in mixed phase structure. The highest electrical conductivity among all mixtures was 1.44×10^{-2} $(\Omega.cm)^{-1}$ at 750 °C for the sample prepared by 1: 1: 1: 2 dopant content ratios. Additionally, we found that the decrease in electrical conductivity may be originated from increase in total dopant ratios, which can negatively effects microstructure, as well as the low polarizability of cations compared to host Bi^{3+} cation. Hence, we concluded that the using multi-doping strategy resulted in lower electrical conductivity than double or triple systems in spite of achieving phase stabilization of the fcc δ-phase. Also, in case of using high doping rate (>50%), we saw that the crystal structure of pure Bi_2O_3 deteriorated due to the occurring different crystal clusters in lattice as a result of doping process. Based on this, we guess that the crystal clusters may lead to peak broadening on the XRD pattern accompanied by the decreasing in average crystal size.

References

[1] Ather H, Syed ZI, Abdul J, et al. Monetization of the environmental damage caused by fossil fuels. Environ. Sci 2021, **28**: 21204–21211.

[2] Imran H. Impact of fossil fuels energy consumption, energy policies, and urban sprawl on carbon emissions in East Asia and the Pacific: A panel investigation. Energy Strategy Rev 2018, **21**: 16-24.

[3] Dokiya M. SOFC system and technology. Solid State Ion 2002, **152**: 383–392.

[4] Mahato N, Banerjee A, Gupta A, *et al*. Progress in material selection for solid oxide fuel cell technology: A review. Prog Mater Sci 2015, **72**: 141–337.

[5] Sammes NM, Tompsett GA, Nafe H, *et al*. Bismuth based oxide electrolytes—structure and ionic conductivity. J Eur Ceram Soc 1999, **19**: 1801–26.

[6] Dapčević A, Poleti D, Rogan J, *et al*. A new electrolyte based on Tm^{3+}-doped δ-Bi2O3-type phase with enhanced conductivity. Solid State Ion 2015, **280**: 18–23.

[7] Sanna S, Esposito V, Andreasen JW, *et al*. Enhancement of the chemical stability in confined δ-Bi2O3. Nat Mater 2015, **14**: 500–504.

[8] Ozlu HT, Cakar S, Ersoy E, *et al.* The bulk electrical conductivity properties of d-Bi2O3 solid electrolyte system doped with Yb2O3. J Therm Anal Calorim 2015, **12**2: 525–536.

[9] Bandyopadhyay S, Dutta A. Thermal, optical and dielectric properties of phase stabilized δ – Dy-Bi2O3 ionic conductors. J Phys Chem Sol 2017, **102**: 12–20.

[10] Polat Y, Dağdemir Y, Arı M. Structural, thermal, electrical and morphological characterization of (Bi2O3)1-x-y(Sm2O3)x(Yb2O3)y nanostructures prepared by solid state synthesis. Curr Appl Phys 2016, **16**: 1588-1596.

[11] Polat Y, Akalan H, Arı M. Thermo-Electrical and Structural Properties of Gd2O3 and Lu2O3 Double-Doped Bi2O3. Int J Hydrogen Energy 2017, **42**: 614-622.

[12] Polat Y, Arı M, Dağdemir Y. Phase stability, thermal, electrical and structural properties of (Bi2O3)1−x−y(Sm2O3)x(CeO2)y electrolytes for solid oxide fuel cells. Phase Transit 2017, **90**: 387-398.

[13] Polat Y. Comments on "Reduced band gap & charge recombination rate in Se doped α-Bi2O3 leads to enhanced photoelectrochemical and photocatalytic performance Theoretical & experimental insight. Int J Hydrogen Energy 2018, **43**: 468-469.

[14] Kış M, Erdoğan B, Polat Y, *et al.* Structural and temperature dependent electrical conductivity properties of Dy2O3 - Sm2O3 co-doped Bi2O3. J Struct Chem 2018, **59**: 1172-1180.

[15] Wachsman E D, Boyapati S, Jiang N. Effect of dopant polarizability on oxygen sublattice order in phase-stabilized cubic bismuth oxides. Ionics 2001, **7**: 1–6.

[16] Dilpuneet S, Aidhy JC, Susan BN, *et al.* Vacancy-Ordered Structure of Cubic Bismuth Oxide from Simulation and Crystallographic Analysis. J Am Ceram Soc 2008, **91**: 2349–2356.

[17] Wachsman ED. Effect of oxygen sublattice order on conductivity in highly defective fluorite oxides. J Eur Ceram Soc 2004, **24**: 1281-1285.

[18] Ahn JS, Camaratta MA, Pergolesi D, *et al.* Development of High Performance Ceria/Bismuth Oxide Bilayered Electrolyte SOFCs for Lower Temperature Operation. J Electrochem Soc 2010, **157**: 376-383.

[19] Jiang N, Wachsman ED, Jung SH. A higher conductivity Bi2O3-based electrolyte. Solid State Ion 2002, **150**: 347–353.

[20] Yilmaz S, Kavici B, Celen C, *et al.* Structure and conductivity characterization of new type ionic conductor stabilized bismuth oxide ternary systems. Chin J Phys 2018, **56**: 362–373.

[21] Arı M, Balcı M, Polat Y. Synthesis and characterization of (Bi2O3)1−x−y−z(Gd2O3)x (Sm2O3)y(Eu2O3)z quaternary solid solutions for solid oxide fuel cell. Chin J Phys 2018, **56**: 2958–2966.

[22] Jung DW, Juan CN, Duncan KL, *et al.* Enhanced long-term stability of bismuth oxide-based electrolytes for operation at 500 °C. Ionics 2010, **16**: 97–103.

[23] Gönen YE, Ermiş I, Ari M. Electrical properties of triple-doped bismuth oxide electrolyte for solid oxide fuel cells. Phase Transit 2015, **89**: 1129–1136.

[24] Ungár T. Microstructural parameters from X-ray diffraction peak broadening. Scripta Materialia 2004, **51**: 777–781.

[25] Vashista M, Paul S. Correlation between full width at half maximum (FWHM) of XRD peak with residual stress on ground surfaces. Philos Mag Lett 2012, **92**: 4194–4204.

[26] Arasteha S, Maghsoudipour A, Alizadeh M, *et al.* Effect of Y2O3 and Er2O3 co-dopants on phase stabilization of bismuth oxide. Ceram Int 2011, **37**: 3451–3455.

[27] Gil V, Tartaj J, Moure C, *et al.* Sintering, microstructural development, and electrical properties of gadolinia-doped ceria electrolyte with bismuth oxide as a sintering aid. J Eur Ceram Soc 2006, **26**: 3161-3171.

[28] Jiang N, Wachsman ED. Structural Stability and Conductivity of Phase-Stabilized Cubic Bismuth Oxides. J Am Ceram Soc 2004, **82**: 57-64.

[29] Krynskia M, Wrobela W, Mohnb CE, *et al.* Abrahams I. Trapping of oxide ions in δ-Bi3YO6. Solid State Ion 2014, **264**: 49-53.

[30] Goodenough JB. Ceramic solid electrolytes. Solid State Ion 1997, **94**: 17-25.

[31] Goodenough JB, Manthiram A, Kuo JF. Oxygen diffusion in perovskite-related oxides. Mater Chem Phys 1993, **35**: 221-224.

[32] Yaremchenkoa AA, Kharton VV, Naumovich EN, *et al.* Stability of δ-Bi2O3-based solid electrolytes. Mater Res Bull 2000, **35**: 515-520.

[33] Azad AM, Larose S, Akbar SA. Bismuth oxide-based solid electrolytes for fuel cells. J Mater Sci 2004, **29**: 4135-4151.

[34] Yun B, Kim KJ, Woo DJ, *et al.* Highly active and durable double-doped bismuth oxide-based oxygen electrodes for reversible solid oxide cells at reduced temperatures. J Mater Chem A 2019, **7**: 20558-20566.

[35] Cardenas PS, Ayala MT, Muñoz J, *et al.* High ionic conductivity dysprosium and tantalum Co-doped bismuth oxide electrolyte for low-temperature SOFCs. Ionics 2020, 26: 4579–4586.

[36] Ruth AL, Lee KT, Clites M, *et al.* Synthesis and Characterization of Double-Doped Bismuth Oxide Electrolytes for Lower Temperature SOFC Application. ECS Trans 2004, **64**: 135-143.

Figure Captions

Fig. 1 The XRD patterns of the annealed samples having various dopant content ratios.

Fig. 2 a) Fwhm and d-spacing variation with respect to average crystal size, b) Lattice microstrain and dislocation density variation with average crystal size for the created samples.

Fig. 3 (a) The electrical conductivity graph depending on temperature for the sample created by 20% total dopant ratio, b) The conductivity comparisons in the certain temperature range for the samples doped by different dopant content ratio.

Fig. 4 (a) The DTA curves depending on temperature for some of the created samples, b) the change in conductivity and activation energy with respect to total dopant ratio.

Fig. 5 The SEM images taken at room temperature for the some created samples having different dopant content ratios.

Table Captions

Table 1 Microstructure parameters revealed from XRD analysis for the annealed samples

Table 2 Electrical characterization results of the annealed pallet samples

Figures

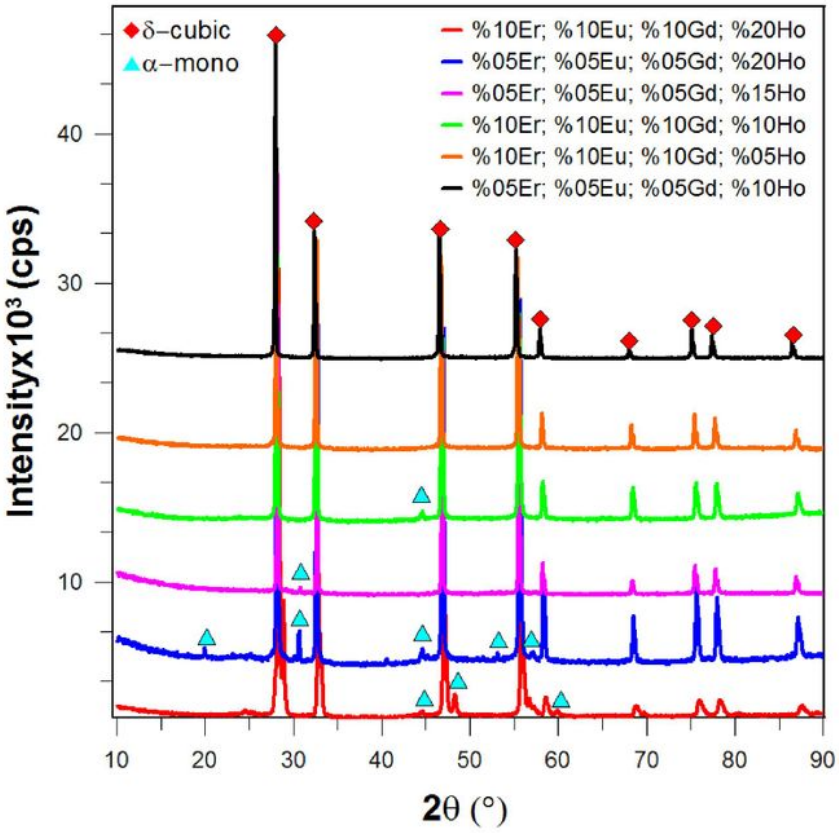

Figure 1

The XRD patterns of the annealed samples having various dopant content ratios.

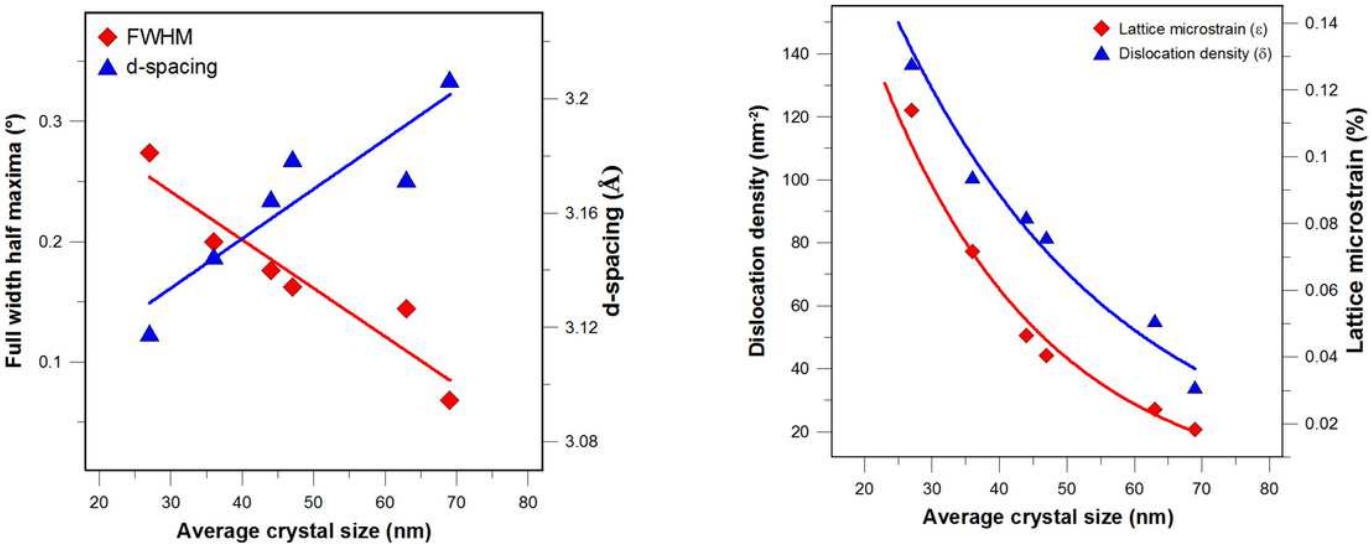

Figure 2

a) Fwhm and d-spacing variation with respect to average crystal size, b) Lattice microstrain and dislocation density variation with average crystal size for the created samples.

Figure 3

(a) The electrical conductivity graph depending on temperature for the sample created by 20% total dopant ratio, b) The conductivity comparisons in the certain temperature range for the samples doped by different dopant content ratio.

Figure 4

(a) The DTA curves depending on temperature for some of the created samples, b) the change in conductivity and activation energy with respect to total dopant ratio.

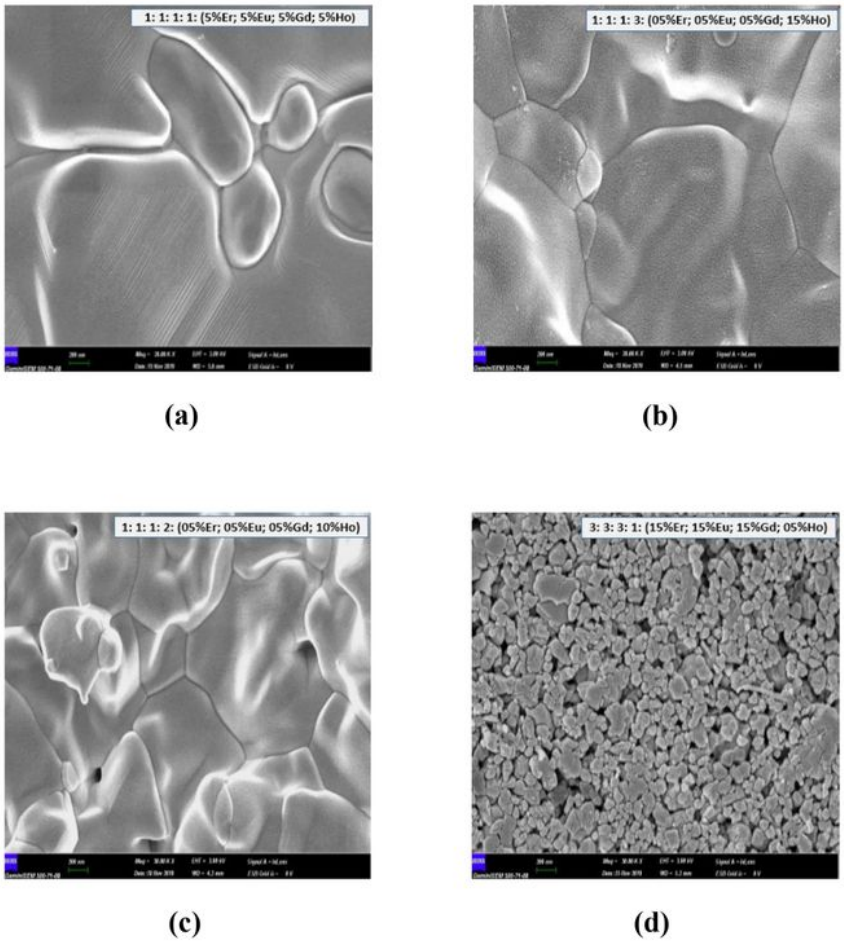

Figure 5

The SEM images taken at room temperature for the some created samples having different dopant content ratios.

Supplementary Files

This is a list of supplementary files associated with this preprint. Click to download.

- Table1..pdf
- Table2.pdf